Disorder and Confinement Effects to Tune the Optical Properties of Amino Acid Doped Cu₂O Crystals

Mariam Kurashvili, Iryna Polishchuk, Arad Lang, Simone Strohmair, Alexander F. Richter, Sebastian Rieger, Tushar Debnath,* Boaz Pokroy,* and Jochen Feldmann*

Biominerals are organic–inorganic nanocomposites exhibiting remarkable properties due to their unique configuration. Using optical spectroscopy and theoretical modeling, it is shown that the optical properties of a model bioinspired system, an inorganic semiconductor host (Cu₂O) grown in the presence of amino acids (AAs), are strongly influenced by the latter. The absorption and photoluminescence excitation spectra of Cu₂O-AAs blue-shift with growing AA content, indicating band gap widening. This is attributed to the void-induced quantum confinement effects. Surprisingly, no such shift occurs in the emission spectra. The theoretical model, assuming an inhomogeneous AA distribution within Cu₂O-AAs due to compositional disorder, explains the deviating behavior of the photoluminescence. The model predicts that the potential causing the confinement effects becomes a function of the local AA density. It results in a Gaussian band gap distribution that shapes the optical properties of Cu₂O-AAs. Imitating and harnessing the process of biomineralization can pave the way toward new functional materials.

1. Introduction

Tuning the optical properties of semiconductors is pivotal in enhancing their functionality and applicability. One crucial way to achieve this is to change the band gap. It can be done, for

M. Kurashvili, S. Strohmair, A. F. Richter, S. Rieger, T. Debnath,
J. Feldmann
Chair for Photonics and Optoelectronics
Nano-Institute Munich and Department of Physics
Ludwig-Maximilians-Universität (LMU)
Königinstr. 10, 80539 Munich, Germany
E-mail: t.debnath@physik.uni-muenchen.de; feldmann@lmu.de
I. Polishchuk, A. Lang, B. Pokroy
Department of Materials Science and Engineering
and the Russell Berrie Nanotechnology Institute
Technion – Israel Institute of Technology
Haifa 32000, Israel
E-mail: bpokroy@tx.technion.ac.il
B. Pokroy
The Nancy and Stephen Grand Technion Energy Program
Technion – Israel Institute of Technology
Haifa 3200003, Israel

example, by altering the chemical composition or by the chemical doping of the semiconductor,[1a–e] altering dimensionality and crystallinity.[1f,g] Recently, followed by numerous studies on the incorporation of various organic molecules into inorganic crystalline hosts,[2] a unique approach for manipulating the band gap of semiconductors inspired by biomineralization has emerged.[3] For example, Pokroy et al. observed that a semiconductor like ZnO grown in the presence of amino acids (AAs) exhibits a significant band gap widening depending on the AA concentration.[3a]

In this work, we show that the optical properties of bioinspired composite Cu₂O-AAs crystals are strongly influenced by the AA content. Cu₂O is a direct band gap semiconductor[4] with a very high exciton binding energy ($\approx$ 150 meV).[5] It has played a crucial role in the development of semiconductor technology[6] and the understanding of important physical phenomena.[7] Owing to its versatility, availability, and numerous application possibilities,[8] Cu₂O is a material of great importance. We find that the incorporation of AAs into the Cu₂O matrix leads to band gap opening, as observed from the blue-shift in the absorption and photoluminescence excitation spectra. We attribute it to void-induced quantum confinement effects.[3b] Surprisingly, such a shift is absent in the emission spectra. We model the absorption spectra of Cu₂O-AAs by combining disorder and confinement effects. The model assumes an inhomogeneous AA arrangement within the crystals due to compositional disorder. Consequently, the potential causing confinement effects becomes a function of the local AA density. It results in a Gaussian band gap distribution that fully reflects the observed optical spectra. Imitating and harnessing the process of biomineralization could pave the way toward new functional materials for optoelectronic applications in, for example, ultrafast switching.

We carried out the synthesis of undoped and AA-doped Cu₂O crystals following our report published earlier.[3c] Briefly, the undoped Cu₂O crystals (**Figure 1**a) were grown without any additive. Cu₂O-AAs were grown by adding glycine and lysine separately (Gly: C₂H₅NO₂, Lys: C₆H₁₄N₂O₂, Figure 1b,c) into the crystallization solution at final concentrations of 3 (Cu₂O-Gly3), 6 (Cu₂O-Gly6) and 10 (Cu₂O-Gly10) of glycine, and 3 (Cu₂O-Lys3) and 6 mg mL⁻¹ (Cu₂O-Lys6) of lysine. After air-drying, the powdered samples were dispersed in ethanol and drop-casted on silica substrates. We examined the Cu₂O-AAs
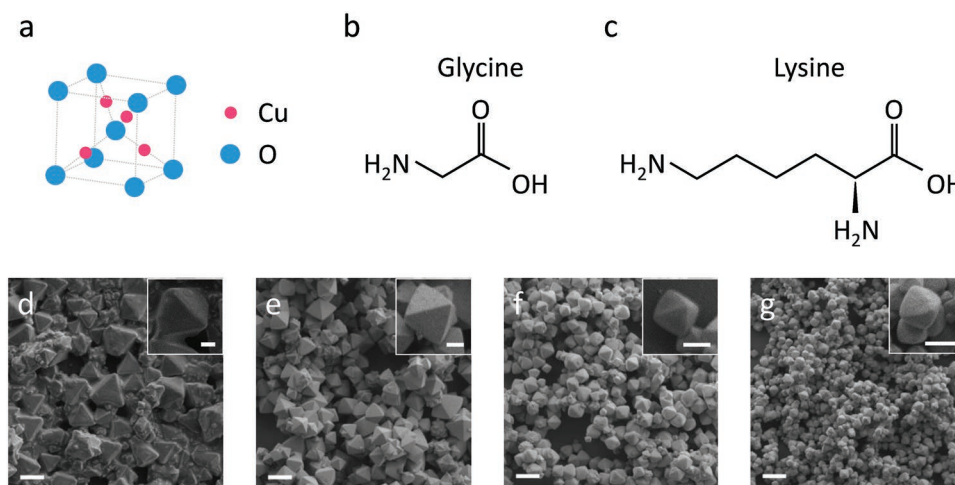
Figure 1. a) A unit cell structure of the Cu₂O crystal. The structural formula of b) glycine and c) lysine. Scanning electron microscopy (SEM) images of d) the undoped Cu₂O, and doped e) Cu₂O-Gly3, f) Cu₂O-Gly6 and g) Cu₂O-Gly10 samples. Scale bar: 3 µm. (Inset) corresponding high-resolution images of one particle. Scale bar: 1 µm.

samples utilizing scanning electron microscopy (SEM), diffuse reflectance (DR), steady-state photoluminescence emission (PL), and photoluminescence excitation (PLE) spectroscopic techniques (see Experimental Section).

2. Results and Discussion

The scanning electron microscopy (SEM) image reveals the undoped Cu₂O sample consists of mostly pyramid-shaped particles (Figure 1d). The particle shape changes upon glycine incorporation from a pyramid to an octahedron (Figure 1d–g insets). In addition, particle size decreases with increasing glycine amount (Figure 1d–g). We determine the edge lengths of the crystals to be 3.02 ± 0.78 µm for the undoped Cu₂O, and 1.98 ± 0.38, 1.23 ± 0.27, and 0.79 ± 0.15 µm for Cu₂O-Gly3, Cu₂O-Gly6, and Cu₂O-Gly10, respectively. Interestingly, not only does the edge length decrease with the increasing incorporation of AAs, but also their spread is reduced indicating that the particle size becomes more regular. Similar changes occur in the case of Cu₂O-Lys samples (Figure S1, Supporting Information). This suggests that incorporation of AAs leads to a modification in the morphology of the Cu₂O host crystals.

The pronounced light scattering effects of our micron-sized particles do not permit any experimental measurements based on the transmission geometry. Therefore, to gain insight into the optical properties of the undoped and AA-doped Cu₂O crystals, we first performed DR measurements (see Experimental Section, Figure S2, Supporting Information). By using the Kubelka–Munk (KM) theory and assuming a limit of an infinitely thick film, we were able to express a frequency-dependent KM function of the samples $F(R_\infty)$ as a function of the measured DR spectra $R_\infty(\nu)$:

$$F(R_\infty) = \frac{\alpha}{S} = \frac{(1-R_\infty)^2}{2R_\infty} \tag{1}$$

which equals the ratio between the frequency-dependent absorption coefficient, $\alpha(\nu)$, and the frequency-independent

scattering constant, S. Hence, the KM function is proportional to the absorption spectrum of the samples.[9] **Figure 2**a,b shows the obtained spectra for several AA doped Cu₂O crystals (see Figure S3a, Supporting Information, for an additional DR related absorption spectrum of Cu₂O-Lys15). The qualitative behavior of the undoped Cu₂O spectrum is in good agreement with the absorption spectrum of Cu₂O reported in the literature.[4,10] Because of the dipole forbidden nature of the $n = 1$ exciton,[11] the DR related absorption spectrum of the undoped Cu₂O does not exhibit a typical exciton peak at ≈1.97 eV but instead a weak shoulder (denoted as "$n = 1$" in Figure 2a).
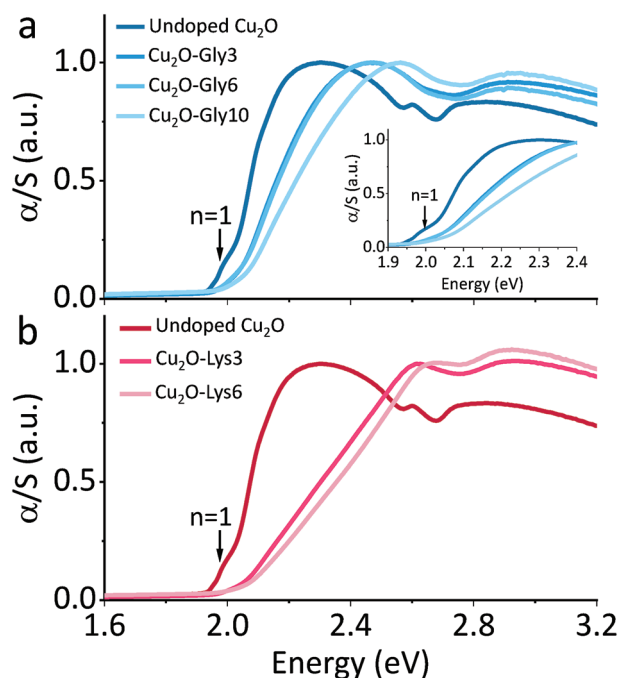

Figure 2. The DR related absorption spectra of the undoped Cu₂O, along with a) Gly-doped crystals and b) Lys-doped crystals. Inset: The expanded DR related absorption spectra of the undoped Cu₂O and Gly-doped crystals for the energy range 1.9–2.4 eV. $n = 1$ marks the exciton position.

ADVANCED
SCIENCE NEWS
www.advancedsciencenews.com

ADVANCED
FUNCTIONAL
MATERIALS
www.afm-journal.de

We find that the DR related absorption spectra of the AA-doped Cu_2O samples, both Cu_2O-Gly and Cu_2O-Lys, are considerably blue-shifted compared to the undoped Cu_2O spectrum. In addition, the higher the AA concentration, the stronger is the observed blue-shift. Qualitatively, this observation agrees with our previous work on AA-doped ZnO crystals, where we reported that the optical band gap of ZnO crystals increases due to the AA-induced quantum confinement effects.[3a,b] In the following, we argue that a similar effect must be at play for Cu_2O-AAs crystals. Quantum confinement effects in Cu_2O start to appear once the particle size decreases below 10 nm.[12] An average distance between the AAs in the doped Cu_2O crystals is estimated by employing solid mass and wavelength dispersive X-ray spectroscopies to be several nanometers long.[3c] Considering the average distance between the AAs and the exciton Bohr radius of Cu_2O (≈ 7 Å),[13] we believe that the doped AAs could act as potential barriers for the excitons and thus, induce quantum confinement, similar to the mechanism reported for the ZnO-AAs composites,[3b] resulting in the blue-shifted absorption spectra. Especially the magnitude of the confinement effects will depend on the distance between the AAs, as previously also demonstrated for ZnO.[3b]

The average separation between the incorporated AAs is several nanometers long. However, the actual distances between the AAs will be distributed inhomogeneously around their average value due to compositional disorder. Consequently, the potential associated with the confinement effects will vary as a function of local AA density. As a result, regions with higher AA concentration will display stronger confinement effects than regions with lower AA concentration. In some AA-scarce regions, the confinement effects might be negligible. Therefore, we argue that the Cu_2O-AAs samples will possess different local band gaps. We expect a normal distribution of the local band gaps around some mean value. Hence, the absorption spectrum of an AA-doped Cu_2O crystal will be a superposition of all local absorption spectra corresponding to the individual crystal regions.

To model the DR related absorption spectra of Cu_2O-AAs, we make several assumptions. We crudely assume that each local absorption spectrum of a certain crystal region $\alpha_{local}(\varepsilon_g, E)$ with a local band gap ε_g strongly resembles the absorption spectrum of the undoped Cu_2O, $\alpha(E_{Cu_2O}, E)$ with a band gap E_{Cu_2O}, except that the local spectrum is blue-shifted with the same magnitude as the local band gap ε_g with respect to E_{Cu_2O}. Here, E represents frequency dependence. The total absorption spectra of the AA-doped samples are weighted sums of the local absorption spectra. The weights are determined by the band gap distribution inside the crystals, $D(\varepsilon_g)$ that we assume to have a Gaussian shape, centered around some mean value ε_{Cu_2O-AA} with a standard deviation σ_{Cu_2O-AA}. Summarizing this as a mathematical expression, we obtain:

$$\alpha_{Cu_2O-AA}(E) = \int_{E_{Cu_2O}}^{\varepsilon_g^{max}} D(\varepsilon_g)\,\alpha_{local}(\varepsilon_g, E)\,d\varepsilon_g \qquad (2)$$

where ε_g^{max} is the largest possible local band gap inside an AA doped crystal. We use $E_{Cu_2O} \approx 2.02\,eV$ as estimated before.[3c]

The orange curves in **Figure 3**a shows the modeled absorption spectra for the Gly-doped samples using Equation (2). The model agrees well with the measured data, especially below 2.6 eV, thus, supporting our initial hypothesis of the inhomogeneous AA distribution within the doped Cu_2O samples. Notably, the model does not predict the absorption spectra for the Cu_2O-Lys (Figure 3b) as accurately as it does for the Cu_2O-Gly crystals. The latter is possible due to more complex band gap distribution function for Lys-doped samples in contrast to the Gly-doped samples, containing an additional NH_2 functional group.

Figure 3c shows the band gap distribution function $D(\varepsilon_g)$ of the AA doped crystals derived from the model. The dashed lines indicate the energy range below $E_{Cu_2O} \approx 2.02\,eV$. The curves in that range do not bear any physical significance because we do not expect any local band gap to be lower than that of the undoped Cu_2O. **Table 1** lists the extracted mean local band gaps ε_{Cu_2O-AA} and the standard deviations of the band gap distributions σ_{Cu_2O-AA} for Cu_2O-Gly and Cu_2O-Lys samples. According to our model, the average local band gap ε_{Cu_2O-AA} of the Cu_2O-AAs samples increases progressively with growing AA content.
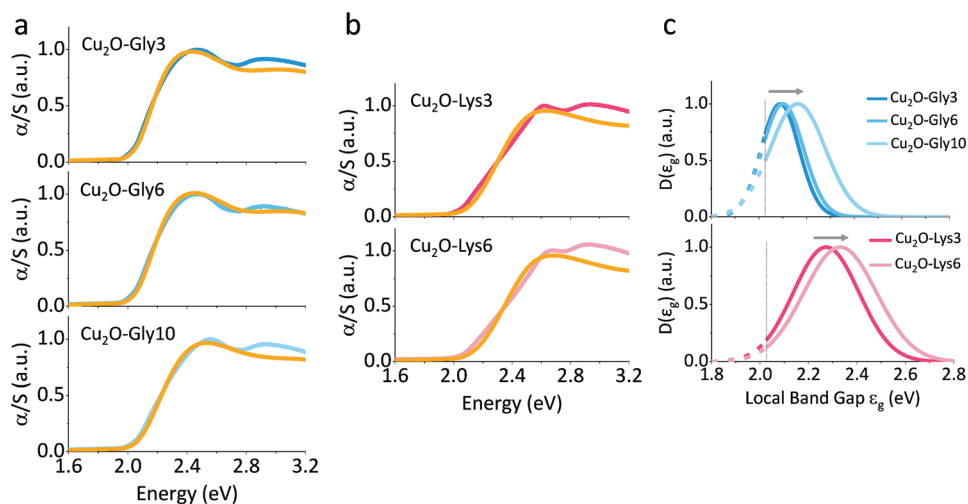

Figure 3. The DR related absorption (blue) and the modeled absorption spectra (orange) using Equation (2) of the doped a) Cu_2O-Gly and b) Cu_2O-Lys. c) The band gap distribution functions for Cu_2O-Gly (above), and Cu_2O-Lys (below) derived from the model. The dashed lines indicate the energies below $E_{Cu_2O} \approx 2.02$ eV (marked by a vertical dotted line). The gray arrows indicate blue-shift.

Table 1. The extracted average local band gaps ε_{Cu_2O-AA} and the standard deviations of the local band gap distributions σ_{Cu_2O-AA} for Gly- and Lys-doped Cu_2O using the model in Equation (2).

Sample	ε_{Cu_2O-AA} [eV]	σ_{Cu_2O-AA} [eV]
Cu_2O-Gly3	2.089	0.079
Cu_2O-Gly6	2.101	0.086
Cu_2O-Gly10	2.163	0.116
Cu_2O-Lys3	2.259	0.135
Cu_2O-Lys6	2.331	0.149

Moreover, the expanding spread of $D(\varepsilon_g)$ as more organic molecules are doped into the Cu_2O crystals reflects a broader local band gap distribution. The model predicts a stronger band gap increase and larger spread in the local band gap distribution functions for Lys-doped samples compared to Gly-doped Cu_2O.

As the incorporated AAs strongly influence the light absorption properties of the Cu_2O crystals, it is of keen interest whether they also change their light emission properties. To this end, we investigated the PL emission spectra of the Cu_2O-AAs samples (see Experimental Section). **Figures 4**a,c compare the obtained spectra for the Gly- and Lys-doped samples, respectively, excited at 510 nm (2.43 eV) (see Figure S3b, Supporting Information, for an additional PL spectrum of Cu_2O-Lys15). In the undoped Cu_2O spectrum, the PL peak ≈2.0 eV stems from the phonon-assisted radiative decay of $n = 1$ excitons.[11a,11b,13,14] The dominant PL peak ≈1.6 eV originates from the emission of excitations at intrinsic defects of Cu_2O.[4,11a,15] Surprisingly, the PL peak positions of the Cu_2O-AAs crystals are very similar to the undoped Cu_2O spectrum (Figure 4a,c), without any blue-shift contrary to the DR related absorption spectra. It is in contrast to our previous observations for ZnO-AAs crystals as well. For those, a blue-shift in the PL relative to the undoped ZnO crystal occurred in both excitonic and defect-assisted emission.[3a,b]

Notably, the exciton emission of the Cu_2O-Gly and -Lys samples broadens, and the typical phonon replica, present in the Cu_2O spectrum, is no longer noticeable (Figure S4, Supporting Information). We believe the broadening of the exciton emission in the AA-doped crystals could be due to decreased exciton–phonon coupling because of the presence of the organic molecules and the resulting compositional disorder. Moreover, a relative increase in the defect to exciton emission as a function of AA content points toward an efficient exciton quenching by the intrinsic and AA-related defect states. Additionally, the time-resolved PL measurements at room temperature (Figure S5, Supporting Information) reveal that although the exciton PL decay for the undoped Cu_2O is very fast (≈5 ps), with growing AA content the decay becomes even faster (e.g., <1 ps for Gly10). We believe, that the decrease in the exciton PL decay times indicates the increase in the number of defect states. The presence of numerous defects states is typical for disordered systems. Thus, we think all this evidence supports our model of inhomogeneous AA distribution within the Cu_2O matrix.

To understand the origin of the PL emission of the Cu_2O-AAs samples, we investigated their PLE spectra. Figure 4b,d depicts the PLE spectra of the composites detected at 1.92 eV. Figure S6, Supporting Information, shows additional PLE spectra detected at different energies. The PLE spectrum of the undoped Cu_2O exhibits a sharp increase starting from ≈1.98 eV. It is in good agreement with the onset of the KM functions of Cu_2O (Figure 2a inset). Thus, for near-band gap excitation energies, we can assume that PLE intensity is proportional to the absorption spectrum. Upon increasing the AA content, we find that the PLE spectra blue-shift progressively, similar to the KM functions. Therefore, both DR related absorption and PLE spectra show blue-shift upon AA incorporation into the Cu_2O matrix, but no blue-shift arises in their corresponding PL spectra.

The question is raised as to why we do not observe a blue-shift in the PL? As our theoretical model revealed, aside from the void-induced quantum confinement, the disorder effects
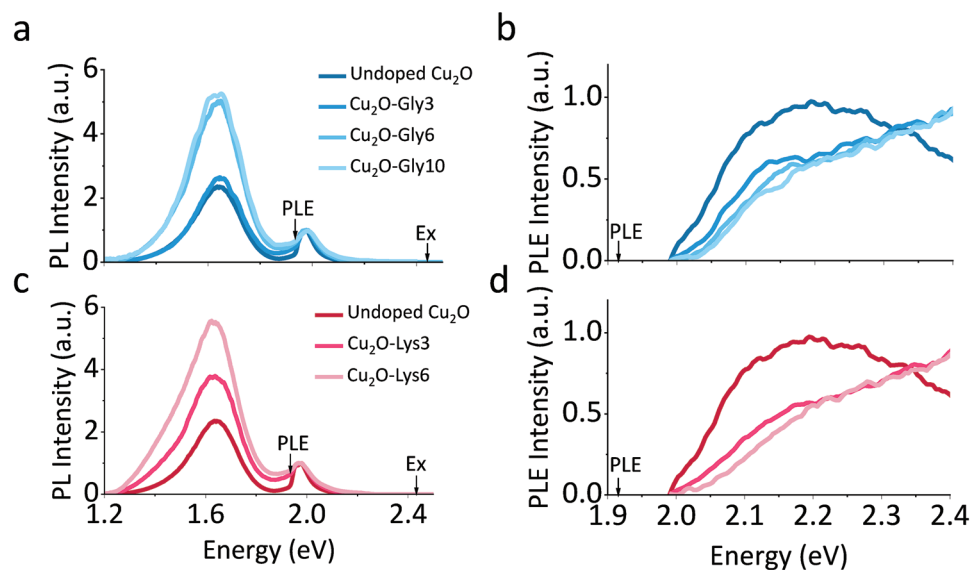

Figure 4. The PL spectra of the undoped Cu_2O along with a) Cu_2O-Gly, and c) Cu_2O-Lys. b,d) The PLE spectra of the same samples as in (a) and in (c), respectively, detected at 1.92 eV.
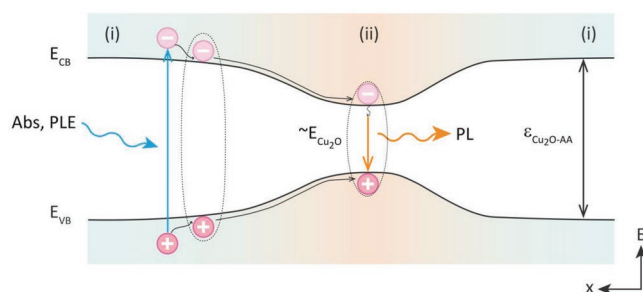
Figure 5. A 1D depiction of the energy band landscape of a Cu_2O-AAs crystal in a one-particle picture. The blue shaded areas (i) denote AA-rich regions. The void-induced quantum confinement effects blue-shift the optical band gap. Their contribution dominates DR related absorption and PLE spectra. The orange shaded area (ii) denotes an AA-poor region. Here, the local crystal environment and electronic structure closely resemble that of the undoped Cu_2O. This region acts as a potential well for excitons. Excitons diffusing to such a region energetically relax inside the potential well and then recombine radiatively. Arrows represent exciton diffusion. Dashed ellipses represent excitons. E_{Cu_2O}–the band gap of the undoped Cu_2O, ε_{Cu_2O-AA} –the average local band gap of the AA-doped Cu_2O.

play a significant role in governing the light absorption behavior of Cu_2O-AAs crystals. Since emission and absorption are related to each other, we expect the disorder effects to have an impact on the latter too. Recall that in an emission process, the excited charge carriers and excitons non-radiatively relax to the lowest excited state before returning to the ground state by releasing a photon. According to the calculated band gap distribution function $D(\varepsilon_g)$, the lowest possible energy where the excitons in the Cu_2O-AAs crystals can relax prior to recombination are located in the AA-poor regions (**Figure 5**). In such regions, the local crystal environment and the local electronic structure will closely resemble those of the undoped Cu_2O, hence serving as potential wells for excitons (Figure 5ii). Excitons diffusing to an AA-poor region will relax energetically into the lower-lying states within the potential wells and then recombine at the local band gap of the undoped Cu_2O. Note, as the AAs act as a barrier, there is a certain energy threshold associated with each barrier that can likely limit the motion of the excitons within the crystal. However, we believe that inside the barriers, there is a non-zero overlap between wavefunctions of excitons, so that the situation becomes analogous to a case of superlattices. Therefore, we believe that AAs do not significantly hinder the exciton motion within the crystals, so that they can diffuse toward the potential wells (local band gap minimum) and relax energetically inside them. This result is consistent with our analysis of the absorption spectra, where we showed that the band gap distribution function $D(\varepsilon_g)$ peaks at higher energies than the band gap of the undoped Cu_2O. We further assess exciton diffusion length L in one dimensions in an undoped Cu_2O using a formula $L = \sqrt{2D\tau}$. Here $D = 10$ cm^2 s^{-1} is the estimated diffusion coefficient of Cu_2O at room temperature[16] and τ is their lifetime. For lifetime as short as 5 ps the diffusion length is 100 nm, which encompasses several hundreds of unit cells. Though the confinement effects and the presence of the AAs might reduce mobility of the excitons in the doped crystals, we strongly believe they will still be able to diffuse over a substantial distance to reach the potential wells.

3. Conclusions

In conclusion, we showed that the incorporation of organic molecules within the Cu_2O crystals strongly influences the optical properties of the latter. The absorption spectra of the Cu_2O-AAs crystals derived from the DR measurements, together with the PLE spectra reveal that their band gaps blue-shift with growing AA content. We attribute it to the AAs acting as barriers for excitons and thus, inducing quantum confinement effects. Surprisingly, no such shift occurs in the PL emission spectra. Our theoretical model provides a crucial step in explaining and consolidating the cumulative observations. The model assumes an inhomogeneous AA distribution within the Cu_2O-AAs crystals due to compositional disorder. Consequently, the potential associated with the confinement effects becomes a function of the local AA density. This results in a Gaussian band gap distribution, which strongly shapes the absorptive and emissive properties of the composites. Our detailed investigation of a model bioinspired system lays the groundwork for new approaches for tuning the optical properties of semiconductors, in particular band gap engineering, which could have potential applications in optoelectronics. Moreover, given the sub-picosecond PL decay rates of the heavily doped specimens, these crystals could find a potential application in terahertz pulse generation.

4. Experimental Section

Synthesis: Copper (II) chloride dehydrate ($CuCl_2\cdot5H_2O$), d-glucose, and sodium hydroxide (NaOH) were purchased from Bio-Lab, Jerusalem, Israel. Cetyltrimethyl ammonium bromide (CTAB) and amino acids (AAs) were purchased from Sigma-Aldrich, St. Louis, MO. 0.057 g $CuCl_2\cdot5H_2O$, 1.093 g of CTAB, 0.079 g d-glucose, and 3 mL NaOH were added to deionized (DI) water in the presence of the L-AAs at various concentrations (L-Glycine: 3 mg mL^{-1}, 6 mg mL^{-1}, 10 mg mL^{-1}. L-Lysine: 3 mg mL^{-1}, 6 mg mL^{-1}). As the initial solutions are alkaline, the AAs are in their fully protonated form (Gly^+ and Lys^{+2}).[3c] The reference sample was prepared without adding any AAs into the aqueous solution. The solutions were transferred into a flask immersed into a silicon oil bath kept at 60 °C, and stirred for 1 h. The resulting Cu_2O crystals were centrifuged, washed with DI water and ethanol several times, and air-dried overnight.

Diffuse Reflectance: To gain an insight into the optical properties of the undoped and AA-doped Cu_2O crystals, the authors first investigated their absorption spectra (optical density, OD) via transmission measurements. The obtained spectra showed nearly constant OD throughout the measured energy range. They attribute this to pronounced light scattering effects of the micron-sized particles. Consequently, the investigated samples did not permit any experimental measurements based on the transmission geometry. Avoiding scattering-susceptible transmission measurements, they performed diffuse DR measurements using a Cary 5000 UV–vis–NIR spectrophotometer (Agilent Technologies, Santa Clara, CA) with a DRA-2500 integrating sphere attachment. The spectra were collected in the visible light range 300–900 nm for the undoped and AA-doped Cu_2O powders (Figure S2, Supporting Information).

Steady-State Photoluminescence Spectroscopy: Steady-state PL measurements were performed by a self-made PL setup. The SuperL Extreme EXR-20 supercontinuum white light laser (WLL) (NKT Photonics) served as a pulsed excitation source with a pulse length ≈5 ps. Its repetition rate was set to 0.304 MHz. The white light laser (WLL) was connected to the acousto-optic tunable filter (AOTF) (NKT Photonics) that enabled selection of the excitation wavelength in the visual (Vis) range. The laser beam exiting the acousto-optic tunable filter

(AOTF) Vis channel was guided on the optical path to the sample with the help of mirrors. A short pass filter (Thorlabs) was used to improve the laser beam quality. A dichroic mirror (Semrock) led the laser beam toward an objective (Olympus SLCPLFL 40x/0.55) that focused the beam on the sample. The dichroic mirror was selected in such a way, that only the PL of the sample was transmitted but not the laser beam reflected back from the sample. An additional long pass filter (Thorlabs) was used to filter out the residual laser light that was able to go through despite the dichroic mirror. The Acton SpectroPro SP2300 spectrometer and a charge coupled device camera PIXIS 400 eXcelon, both from Princeton Instruments were used to record the spectra.

PLE spectroscopy was an experimental technique suited for gaining insight into the electronic band structure. PLE intensity I_{PLE} is proportional to the product of the probability of absorption P_{abs}, relaxation into the respective emissive states P_{rel}, and emission P_{em}: $I_{PLE} \approx P_{abs} P_{rel} P_{em}$. PLE spectra were measured with the same setup as the PL spectra. All emission intensities detected at various excitation energies were normalized by the corresponding average power of the incoming laser pulse. In order to render the PLE spectra of different samples comparable to each other the following treatments were performed: the lowest intensity was set to zero and the highest intensity to one. The rest was scaled linearly. The spectra were smoothed using a binomial signal processing method. This adjustment did not change the information contained in the PLE spectra.

Time-Resolved Photoluminescence Spectroscopy: The authors recorded time-resolved PL spectra using a universal streak camera C10910 with an attached synchroscan unit M10911 and an ORCA-Flash4.0 V3 digital complementary metal-oxide-semiconductor camera, all from Hamamatsu. They used a spectrograph SpectraPro HRS-300 from Princeton Instruments to resolve the wavelengths. A MIRA 900 Ti:sapphire laser (MIRA), pumped by a Verdi V10 DPSS laser at 532 nm (both from Coherent), was used as a pump source for optical parametric oscillator (OPO) by APE. The excitation laser pulse length was $\tau_{pulse} \approx 100$ fs, the repetition frequency was set to $f_{rep} = 75.6$ MHz, and the excitation wavelength was set to 565 nm. The excitation power was selected in a way to avoid many-body effects. The laser beam was guided on the optical path by the mirrors and focused on the sample by a lens. Finally, the resulting PL was focused on the entrance slit of the spectrograph. The residual laser light was filtered out by a long pass filter 600 nm from Thorlabs, placed just prior to the entrance slit of the spectrograph. A delay system C12270 from Hamamtsu was used to synchronize the beam phase between MIRA and the synchroscan unit of the streak camera.

Theoretical Modeling: Theoretical modeling as described in the main text was performed in Matlab R2019a. The lowest value ε_{Cu_2O-AA} was allowed to take was E_{Cu_2O}. The upper limit was varied. The band gap values previously calculated by Polishchuk et al.[3c] served as a guideline when selecting the value of ε_{Cu_2O-AA}. During the initial fit σ_{Cu_2O-AA} was allowed to vary while ε_{Cu_2O-AA} was kept fixed. Afterward σ_{Cu_2O-AA} was set to the fitted value and ε_{Cu_2O-AA} was allowed to vary. This process was repeated several times manually in order to obtain the best fit to the data in the range 1.8–2.5 eV ($R^2 \geq 0.97$). Additionally, the amplitude of the Gaussian band gap distribution function $D(\varepsilon)$ was allowed to vary. This was necessary in order to ensure correct normalization of the model with respect to the experimental data. The distribution functions reported in Figure 3c are normalized.

Supporting Information

Supporting Information is available from the Wiley Online Library or from the author.

Conflict of Interest

The authors declare no conflict of interest.

Data Availability Statement

The data that support the findings of this study are available from the corresponding author upon reasonable request.

[1] a) A. Ohtomo, M. Kawasaki, T. Koida, K. Masubuchi, H. Koinuma, Y. Sakurai, Y. Yoshida, T. Yasuda, Y. Segawa, *Appl. Phys. Lett.* **1998**, *72*, 2466; b) S. C. Das, R. J. Green, J. Podder, T. Z. Regier, G. S. Chang, A. Moewes, *J. Phys. Chem. C* **2013**, *117*, 12745; c) A. Janotti, C. G. Van de Walle, *Rep. Prog. Phys.* **2009**, *72*, 126501; d) C. Hu, T. Ye, Y. Liu, J. Ren, X. Jin, H. Chen, H. Li, *Mater. Chem. Front.* **2018**, *2*, 362; e) L. Yang, Y. Peng, Y. Yang, J. Liu, H. Huang, B. Yu, J. Zhao, Y. Lu, Z. Huang, Z. Li, J. R. Lombardi, *Adv. Sci.* **2019**, *6*, 1900310; f) X. Wang, W. Shi, S. Wang, H. Zhao, J. Lin, Z. Yang, M. Chen, L. Guo, *J. Am. Chem. Soc.* **2019**, *141*, 5856; g) A. Li, J. Yu, J. Lin, M. Chen, X. Wang, L. Guo, *J. Phys. Chem. Lett.* **2020**, *11*, 1859.

[2] a) S. Borukhin, L. Bloch, T. Radlauer, A. H. Hill, A. N. Fitch, B. Pokroy, *Adv. Funct. Mater.* **2012**, *22*, 4216; b) Y. Y. Kim, J. D. Carloni, B. Demarchi, D. Sparks, D. G. Reid, M. E. Kunitake, C. C. Tang, M. J. Duer, C. L. Freeman, B. Pokroy, K. Penkman, J. H. Harding, L. A. Estroff, S. P. Baker, F. C. Meldrum, *Nat. Mater.* **2016**, *15*, 903; c) Y. Y. Kim, K. Ganesan, P. Yang, A. N. Kulak, S. Borukhin, S. Pechook, L. Ribeiro, R. Kroger, S. J. Eichhorn, S. P. Armes, B. Pokroy, F. C. Meldrum, *Nat. Mater.* **2011**, *10*, 890; d) D. C. Green, R. Darkins, B. Marzec, M. A. Holden, I. J. Ford, S. W. Botchway, B. Kahr, D. M. Duffy, F. C. Meldrum, *Cryst. Growth Des.* **2021**, *21*, 3746; e) O. Nahi, A. N. Kulak, T. Kress, Y. Y. Kim, O. G. Grendal, M. J. Duer, O. J. Cayre, F. C. Meldrum, *Chem. Sci.* **2021**, *12*, 9839.

[3] a) A. Brif, G. Ankonina, C. Drathen, B. Pokroy, *Adv. Mater.* **2014**, *26*, 477; b) M. A. H. Muhammed, M. Lamers, V. Baumann, P. Dey, A. J. Blanch, I. Polishchuk, X.-T. Kong, D. Levy, A. S. Urban, A. O. Govorov, B. Pokroy, J. Rodríguez-Fernández, J. Feldmann, *J. Phys. Chem. C* **2018**, *122*, 6348; c) I. Polishchuk, N. Bianco-Stein, A. Lang, M. Kurashvili, M. C. Toroker, A. Katsman, J. Feldmann, B. Pokroy, *Adv. Funct. Mater.* **2020**, *30*, 1910405; d) A. Brif, L. Bloch, B. Pokroy, *CrystEngComm* **2014**, *16*, 3268; e) A. Lang, I. Polishchuk, E. Seknazi, J. Feldmann, A. Katsman, B. Pokroy, *Adv. Funct. Mater.* **2020**, *30*, 2005136.

**ADVANCED
SCIENCE NEWS**

www.advancedsciencenews.com

**ADVANCED
FUNCTIONAL
MATERIALS**

www.afm-journal.de

[4] B. K. Meyer, A. Polity, D. Reppin, M. Becker, P. Hering, P. J. Klar, T. Sander, C. Reindl, J. Benz, M. Eickhoff, C. Heiliger, M. Heinemann, J. Blasing, A. Krost, S. Shokovets, C. Muller, C. Ronning, *Phys. Status Solidi B* **2012**, *249*, 1487.

[5] D. W. Snoke, D. Braun, M. Cardona, *Phys. Rev. B: Condens. Matter Mater. Phys.* **1991**, *44*, 2991.

[6] L. O. Grondahl, P. H. Geiger, *J. A.I.E.E.* **1927**, *46*, 215.

[7] a) E. F. Gross, *Nuovo Cimento* **1956**, *3*, 672; b) D. Hulin, A. Mysyrowicz, C. Benoît à la Guillaume, *Phys. Rev. Lett.* **1980**, *45*, 1970.

[8] a) D. J. Kim, H. J. Kim, K. W. Seo, K. H. Kim, T. W. Kim, H. K. Kim, *Sci. Rep.* **2015**, *5*, 16838; b) Q. L. Liu, H. J. Tian, J. W. Li, A. Q. Hu, X. Y. He, M. L. Sui, X. Guo, *Adv. Opt. Mater.* **2019**, *7*, 1900455; c) J. Luo, L. Steier, M. K. Son, M. Schreier, M. T. Mayer, M. Gratzel, *Nano Lett.* **2016**, *16*, 1848; d) L. L. Wan, Q. X. Zhou, X. Wang, T. E. Wood, L. Wang, P. N. Duchesne, J. L. Guo, X. L. Yan, M. K. Xia, Y. F. Lie, A. A. Jelle, U. Ulmer, J. Jia, T. Li, W. Sun, G. A. Ozin, *Nat. Catal.* **2019**, *2*, 889.

[9] a) J. P. Blitz, in *Modern Techniques in Applied Molecular Spectroscopy: Techniques in Analytical Chemistry* (Ed: F. M. Mirabella), John Wiley & Sons, New York **1998**, p. 185, Ch. 5; b) R. Alcaraz de la Osa, I. Iparragirre, D. Ortiz, J. M. Saiz, *ChemTexts* **2020**, *6*, 2.

[10] C. Malerba, F. Biccari, C. L. A. Ricardo, M. D'Incau, P. Scardi, A. Mittiga, *Sol. Energy Mater. Sol. Cells* **2011**, *95*, 2848.

[11] a) T. Ito, T. Masumi, *J. Phys. Soc. Jpn.* **1997**, *66*, 2185; b) R. J. Elliott, *Phys. Rev.* **1961**, *124*, 340; c) T. Kazimierczuk, D. Fröhlich, S. Scheel, H. Stolz, M. Bayer, *Nature* **2014**, *514*, 343. d) P. Y. Yu, Y. R. Shen, *Phys. Rev. B* **1975**, *12*, 1377.

[12] P. Poulopoulos, S. Baskoutas, S. D. Pappas, C. S. Garoufalis, S. A. Droulias, A. Zamani, V. Kapaklis, *J. Phys. Chem. C* **2011**, *115*, 14839.

[13] D. W. Snoke, A. J. Shields, M. Cardona, *Phys. Rev. B: Condens. Matter Mater. Phys.* **1992**, *45*, 11693.

[14] a) J. Q. Li, Z. X. Mei, D. Q. Ye, H. L. Liang, L. S. Liu, Y. P. Liu, A. Galeckas, A. Y. Kuznetsov, X. L. Du, *Opt. Mater. Express* **2013**, *3*, 2072; b) A. Compaan, H. Z. Cummins, *Phys. Rev. B* **1972**, *6*, 4753; c) Y. Petroff, P. Y. Yu, Y. R. Shen, *Phys. Rev. B* **1975**, *12*, 2488; d) A. Compaan, H. Z. Cummins, *Phys. Rev. Lett.* **1973**, *31*, 41.

[15] S. V. Gastev, A. A. Kaplyanskii, N. S. Sokolov, *Solid State Commun.* **1982**, *42*, 389.

[16] F. Biccari, C. Malerba, A. Mittiga, *Sol. Energy Mater. Sol. Cells* **2010**, *94*, 1947.